NANO · MICRO small
www.small-journal.com

Tunable Molecular Electrodes for Bistable Polarization Screening

Irena Spasojevic, José Santiso, José Manuel Caicedo, Gustau Catalan, and Neus Domingo**

The polar discontinuity at any ferroelectric surface creates a depolarizing field that must be screened for the polarization to be stable. In capacitors, screening is done by the electrodes, while in bare ferroelectric surfaces it is typically accomplished by atmospheric adsorbates. Although chemisorbed species can have even better screening efficiency than conventional electrodes, they are subject to unpredictable environmental fluctuations and, moreover, dominant charged species favor one polarity over the opposite. This paper proposes a new screening concept, namely surface functionalization with resonance-hybrid molecules, which combines the predictability and bipolarity of conventional electrodes with the screening efficiency of adsorbates. Thin films of barium titanate ($BaTiO_3$) coated with resonant para-aminobenzoic acid (pABA) display increased coercivity for both signs of ferroelectric polarization irrespective of the molecular layer thickness, thanks to the ability of these molecules to swap between different electronic configurations and adapt their surface charge density to the screening needs of the ferroelectric underneath. Because electron delocalization is only in the vertical direction, unlike conventional metals, chemical electrodes allow writing localized domains of different polarity underneath the same electrode. In addition, hybrid capacitors composed of graphene/pABA/ferroelectric have been made with enhanced coercivity compared to pure graphene-electode capacitors.

1. Introduction

The polar discontinuity at ferroelectric surfaces and concomitant presence of a detrimental depolarization field can be mitigated in several ways. One is the formation of domains. Another is the provision of screening charge, supplied internally in the form of free charge-carriers, externally by metallic electrodes, or, in the case of bare (electrode-free samples), by adsorbate species (**Figure 1**a). External screening by adsorbates coming from the atmosphere (such as H_2O and O_2)[1–5] has been shown to be more effective in stabilizing the ferroelectric phase compared to metallic electrodes with finite screening length.[6]

Atmospheric adsorbates cannot be considered the most optimal screening species because: i) Their composition and adsorption is difficult to control and predict, sometimes leading to undesirable effects such as sample degradation,[7] dependence on sample's history[8] or polarization switching[4,5,9–11] and ii) The charge sign or preferred dipole orientation of screening species tends to stabilize one ferroelectric polarity over the opposite, i.e., screening species can be considered as unipolar, requiring the dipole rotation and change of the interfacial chemical bond upon switching.[12]

In view of this, it is desirable to find a screening mechanism that combines the screening efficiency of chemical adsorbates with the predictability and bipolar screening ability of metallic electrodes. The strategy we propose is the chemical modification of ferroelectric surfaces by functionalization with optimal screening molecules. In order to be considered optimal, such "chemical electrodes" have to meet several requirements: i) to provide efficient electrical screening of depolarization fields, so that ferroelectric polarization is stable, ii) to be able to adapt to the change in screening needs upon polarization reversal, so that polarization can be switched. In addition, and from a practical point of view, the availability of the material and its suitability for nanofabrication must be considered. As will be shown, all these criteria are met by para-aminobenzoic acid.

In this work we demonstrate the effective bipolar stabilization of ferroelectricity in hybrid organic–ferroelectric heterostructures based on the functionalization of $BaTiO_3$ (BTO) with pABA molecules. pABA molecules exhibit high degree of delocalization of electrons throughout the benzene ring and its carboxylic and amino group substituents.[13] In addition, pABA

I. Spasojevic, J. Santiso, J. M. Caicedo, G. Catalan, N. Domingo[+]
Catalan Institute of Nanoscience and Nanotechnology (ICN2)
CSIC and BIST
Campus UAB, Bellaterra, Barcelona 08193, Spain
E-mail: Irena.Spasojevic@uab.cat; ndomingo@ornl.gov
I. Spasojevic
Department of Chemistry
Universitat Autònoma de Barcelona
Bellaterra, Barcelona 08193, Spain
G. Catalan
ICREA- Institució Catalana de Recerca i Estudis Avançats
Catalonia, Barcelona 08010, Catalonia
The ORCID identification number(s) for the author(s) of this article can be found under https://doi.org/10.1002/smll.202207799.

[+]Present address: Center for Nanophase Materials Sciences, Oak Ridge National Laboratory, Oak Ridge, TN 37830, USA

DOI: 10.1002/smll.202207799

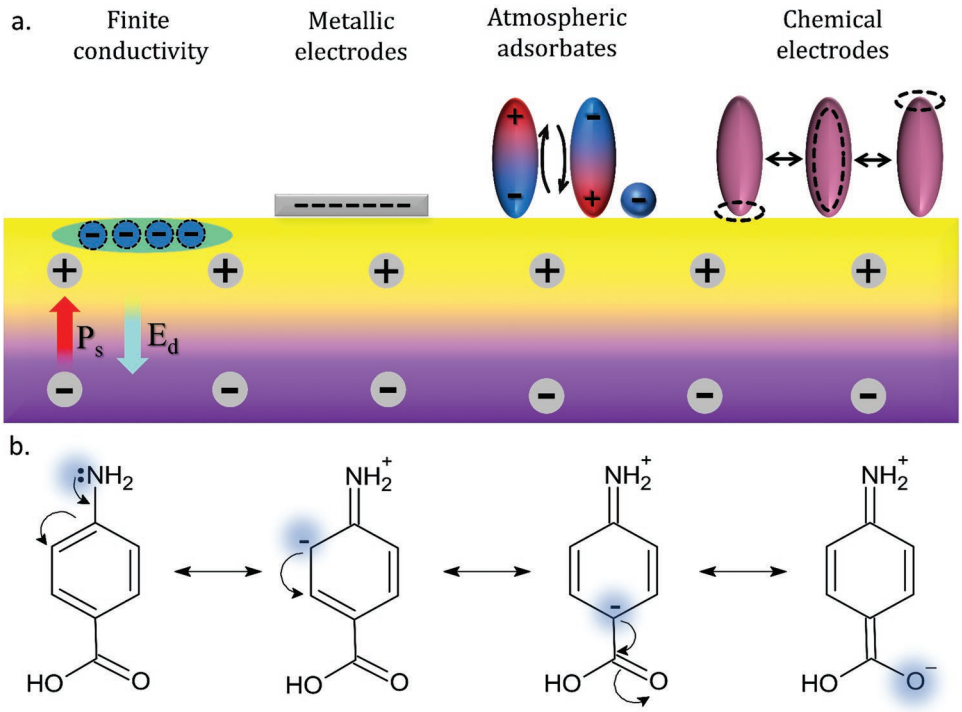

Figure 1. a) Screening mechanisms of a monodomain ferroelectric material, which include (from left to right) internal screening by free charge carriers and external screening by metallic electrodes or atmospheric adsorbates. The last one is screening by molecules with a delocalized electronic system able to internally relocate the electrons, i.e., chemical electrodes. Electrons' relocation should be highly sensitive and specific to the polarization direction and bound polarization charge of the underneath ferroelectric substrate; b) some resonance structures (electronic configurations) of pABA molecule proposed in this work, contributing to the resonance hybrid. A blue cloud represents the location of negative charge carriers.

molecules possess distinct configurations ("chemical resonance") whereby the electrons can be internally relocated along the out-of-plane direction and thus tune the surface charge density without changing their chemical configuration/surface bonding as shown in (Figure 1b). The free amino ($-NH_2$) group is an electron donor able to couple its lone electron pair with the high electron density of the benzene ring and further with the lone electron pairs of oxygen atoms in the carboxylic (COOH) group,[14] enabling electrons to be fully delocalized. The structure of pABA delocalized electronic system is depicted by the resonance hybrid,[13,15] representing weighted averaged contribution of several resonance structures with distinct electrons' distribution within the molecule which, as shown in Figure 1, may act as a counterweight to the bipolar depolarization fields of ferroelectrics: upward polarization should attract the delocalized electrons towards the BTO surface; conversely, downward polarization should repel the delocalized electrons further from the surface towards the benzene ring. Furthermore, we probe the screening efficiency of pABA molecules in capacitor-like geometry, build up from pABA functionalized BTO thin films sandwiched between $SrRuO_3$ (SRO) bottom and multilayer graphene top electrode.

2. Results and Discussion

2.1. Functionalization of BTO Thin Films with pABA Molecules

Epitaxial ferroelectric BTO/SRO bilayers were grown by Pulsed Laser Deposition (PLD) technique on as received (100) oriented $SrTiO_3$ (STO) single crystalline substrates (CrysTec GmbH). Growth parameters and detailed preparation procedure can be found elsewhere.[4] The structural characterization of BTO/SRO bilayers is shown in Figure S1 (Supporting Information).

Controlled nanopatterning of BTO thin films by pABA molecules was performed by microcontact printing (μCP) method, by brining polydimethylsiloxane (PDMS) stamp inked by pABA molecules into conformal contact with BTO thin film as shown in **Figure 2**a. The atomic force microscopy (AFM) topography of pABA molecules on micropatterned BTO sample is shown in Figure 2b. From the topography image, the presence of molecules in the perimeter of the square-like reliefs is evident, however it is not clear whether there are some molecular layers also inside or outside the square-like patterns. In order to determine the presence of pABA molecules on BTO surfaces we employed Kelvin Probe Force Microscopy (KPFM) and Amplitude Modulated Frequency Modulated (AM-FM) Viscoelastic Mapping.

The contact potential difference image obtained by KPFM is plotted in Figure 2c. The observed contrast between inner and outer regions of square-like features is consistent with different chemical composition of these two areas of the surface, corresponding to bare BTO surface and pABA-functionalized BTO surface. In addition, the Young's modulus and indentation of the material was obtained from AM-FM viscoelastic mapping and shown in Figure 2d,e, respectively. The area surrounding the square-like features exhibits lower Young modulus (Figure 2d) and higher indentation values as compared to their inner area, indicating the presence of soft molecules compared to bare

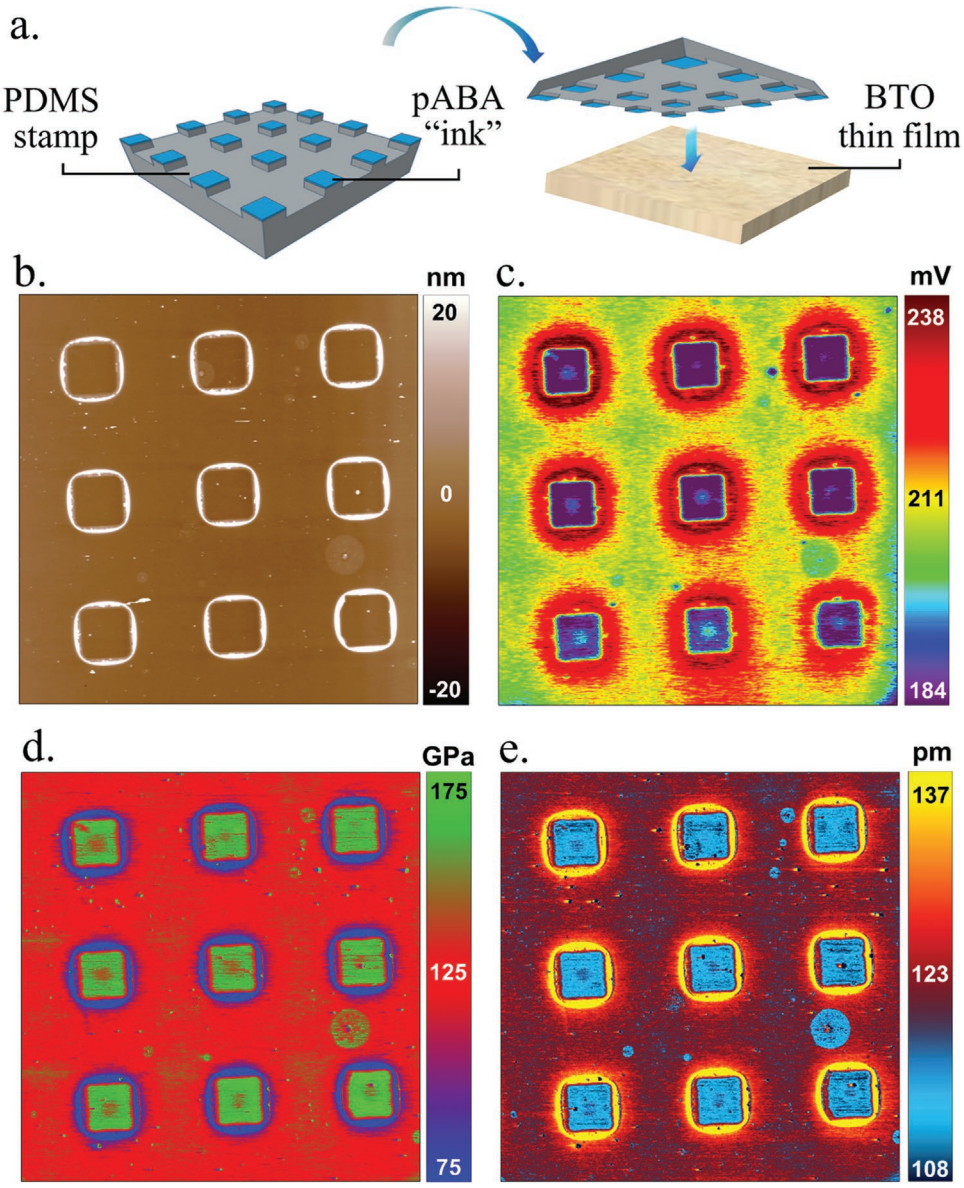

Figure 2. a) Schematic representation of microcontact printing process (top); AFM imaging of microcontact printed patterns of pABA molecules on a BTO thin film (bottom) such as b) AFM tapping mode topography; c) contact potential difference as measured by KPFM; d) Young's modulus and e) indentation obtained by AM-FM Viscoelastic Mapping. AFM images have dimensions of 45 µm × 45 µm. Detailed explanation of images can be found in the main text.

BTO. The evidence thus indicates that the BTO surface inside the squares is bare while pABA molecules cover the rest of the film around the patterned squares. Furthermore, infrared characterization indicates that pABA molecules chemically attach to the BTO surface by forming ester-like monodentate linkage with Ti atoms (Figure S2, Supporting Information), which is in agreement with studies of pABA functionalized TiO_2 surfaces.[16,17]

2.2. Coupling of pABA Molecules and Ferroelectric Polarization in BTO Thin Films

In order to explore the impact of pABA surface-chemical modification on the ferroelectric properties of BTO thin films, we used Piezoresponse Force Microscopy (PFM). **Figure 3** shows topography, PFM phase images and PFM hysteresis loops (of PFM phase as a function of voltage) for as-grown BTO film with naturally present atmospheric adsorbates (Figure 3a–c), non-functionalized (i.e., bare) area of BTO film (Figure 3d–f) and pABA-functionalized area of the same BTO thin film (Figure 3g–i).

A defining characteristic of ferroelectric materials is that their spontaneous ferroelectric polarization can be reversed by the application of an external electric field. Figure 3b shows the PFM phase image of electrically-written ferroelectric domains. In this case ferroelectric lithography is done by applying a DC voltage of +8 and −8 V to the tip while scanning in contact over square like areas denoted by black lines,

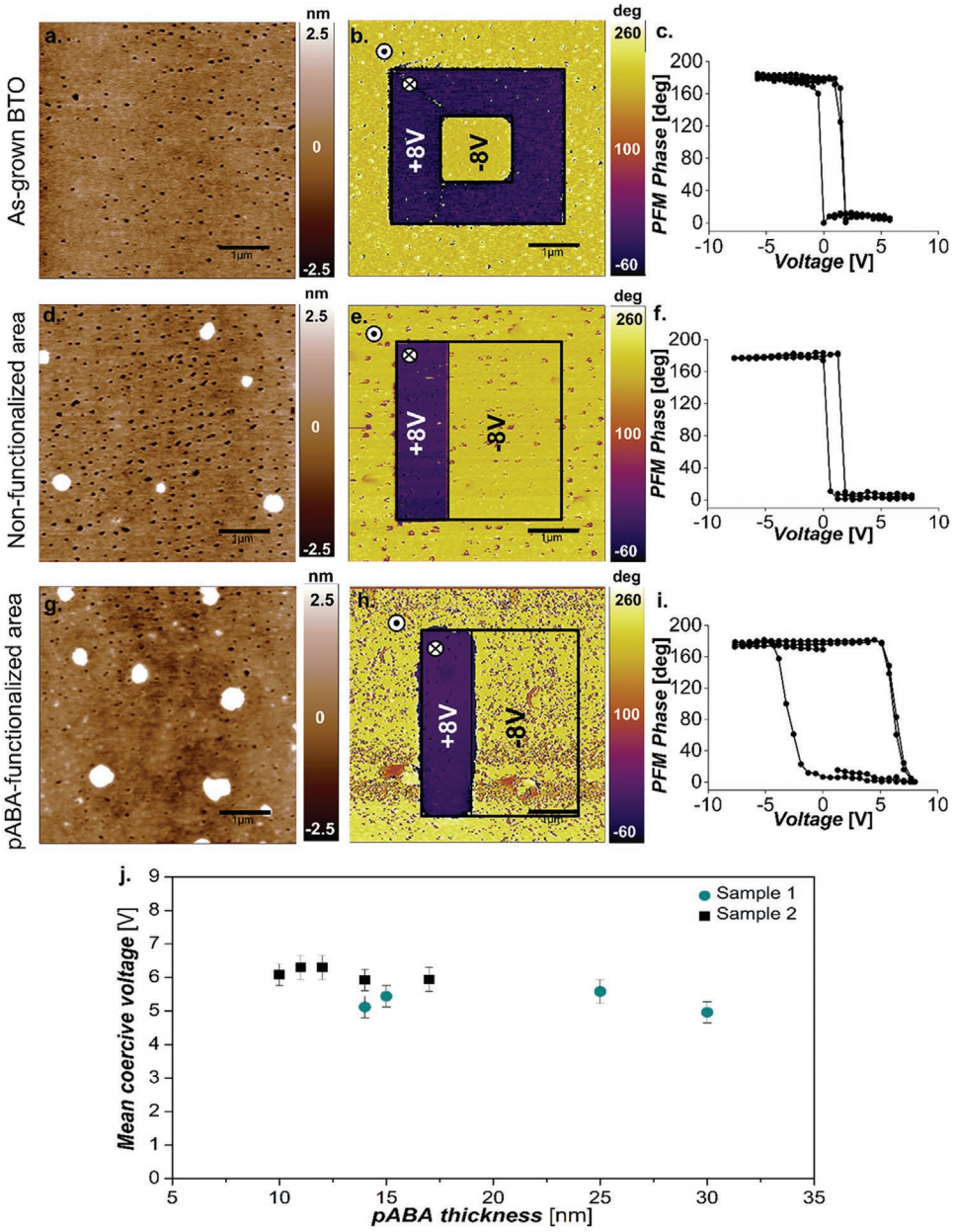

Figure 3. Ferroelectric characterization of as-grown BTO film with naturally present atmospheric adsorbates, non-functionalized (bare) area of BTO film and pABA-functionalized area of the same BTO film; AFM topography image of a) as-grown BTO, d) non-functionalized and g) pABA-functionalized area of the same BTO thin film; PFM phase images of electrically written ferroelectric domains, by applying DC voltages of +8 and −8 V to the AFM tip while scanning areas denoted by black lines in contact with b) as-grown BTO, e) non-functionalized and h) pABA-functionalized area of BTO thin film. From the phase contrast of PFM phase images, it can be seen that BTO film is up-polarized in all three cases; SS-PFM hysteresis loops of PFM phase obtained on c) as-grown, f) non-functionalized and i) pABA-functionalized area of BTO thin film, where a drastic increase of the coercive voltage can be observed; j) Mean coercive voltage $V = (|V_{c-}| + |V_{c+}|)/2$ as a function of pABA layer thickness for two BTO samples.

obtaining downward and upward polarized states, respectively. Phase-contrast images show that the as-grown BTO thin film is spontaneously up-polarized, which is typical for BTO films grown on SRO-buffered STO substrates.[6] The hysteresis loop of the as-grown BTO sample screened by atmospheric adsorbates reveals a mean coercive voltage of $V = 1$ V and $V_{bias} = +0.6$ V. The observed asymmetry of the loop, shifted to positive voltages, agrees with the preferential up-polarized state of the BTO film. Ferroelectric properties measured on the non-functionalized area of pABA-modified BTO thin film do not change significantly as compared to as-grown BTO as shown in Figure 3e,f. Finally, pABA-functionalized area of BTO film keeps its as-grown up-polarized state (Figure 3h), however, a drastic widening of PFM hysteresis loops of the hybrid organic–inorganic pABA/BTO heterostructure is observed, with a substantial enhancement of the mean coercivity up to $V = 6.1$ V and $V_{bias} = +1.5$ V (Figure 3i,j).

First, we consider whether the observed enhancement of the coercive field may be caused by a trivial passive-layer effect, whereby the pABA molecules act as a layer of low dielectric constant connected in series with the underneath ferroelectric. The presence of such passive layer would affect the electric field sensed by the sample and therefore the measured coercive voltage, which would be linearly proportional to the thickness of the passive layer. Figure 3g shows the dependence of the mean coercive voltage ($V_c = |V_{c-}| + |V_{c+}|)/2$) on the pABA molecular layer thickness as measured by switching spectroscopy PFM (SS-PFM) for two BTO samples. For both samples, hysteresis loops were probed in several different positions corresponding to different thicknesses of the pABA molecular layer as measured from AFM topography height profiles (Figure S3, Supporting Information). Figure 3g shows that the coercive voltage is essentially the same for both samples and independent of the pABA layer thickness. Hence pABA molecules do not contribute to an increase of the coercive voltage as a dielectric "passive layer".

Instead, the increased coercive voltage is consistent with an enhancement of the stability of both up and down polarization states thanks to an effective suppression of the depolarizing fields.[18] In this context, pABA molecules act as an electroactive layer that is able to supply/take negative charges from the surface region as dictated by the polarization of the underneath film, and provide a superior screening for both signs of the ferroelectric polarization (hence bistability) compared to naturally present "unipolar" atmospheric adsorbates.

In the case of up-polarized ferroelectric state which requires negative screening charge, delocalized electrons from electro-donating amino group and benzene ring are attracted toward the carboxylic group and act as additional negative screening agents in the vicinity of the surface (**Figure 4** left). Oppositely, down-polarized BTO thin films will repel negative charges in the vicinity of the surface and delocalize the electrons inside of benzene ring in order to achieve more positive ferroelectric screening (Figure 4 right).

It has been reported that inorganic molecules physisorbed on ferroelectric surfaces such as NH_3 are able to rotate upon polarization reversal and therefore bring their electropositive (hydrogen) or electronegative (nitrogen) atoms closer or further from ferroelectric surfaces.[12] However, in our case pABA molecules are chemisorbed, which makes it impossible for them to rotate; instead it is the internal electronic density that moves along delocalized bonds in order to compensate the bound charge of the ferroelectric surface, thus resulting in a more robust ferroelectric polarization. This result is further supported by Kelvin Probe Force Microscopy measurements of pABA-functionalized up- and down-polarized BTO thin films showing the different polarity of the charge concentration close to the molecular surface for both cases (Figure S5, Supporting Information).

Since this screening mechanism comprises fast internal relocation of delocalized electrons instead of slow dipole reorientation, we expect a faster speed at which ferroelectric polarization can be screened and therefore switched. Moreover, as observed from Figure 3e, electron delocalization happens only in the out-of-plane direction (i.e., along the vertical axis of pABA molecules), while the in-plane direction remains sufficiently insulating to ensure that the switching happens only under the writing tip and not under the entire pABA layer. This offers an advantage of pABA tunable chemical electrodes over conventional metallic electrodes where the size of the written domains is predetermined by the lateral extension of the top electrode and its in-plane conductivity. With molecular-based screening, one can even write localized domains of different polarity under the same chemical electrode.

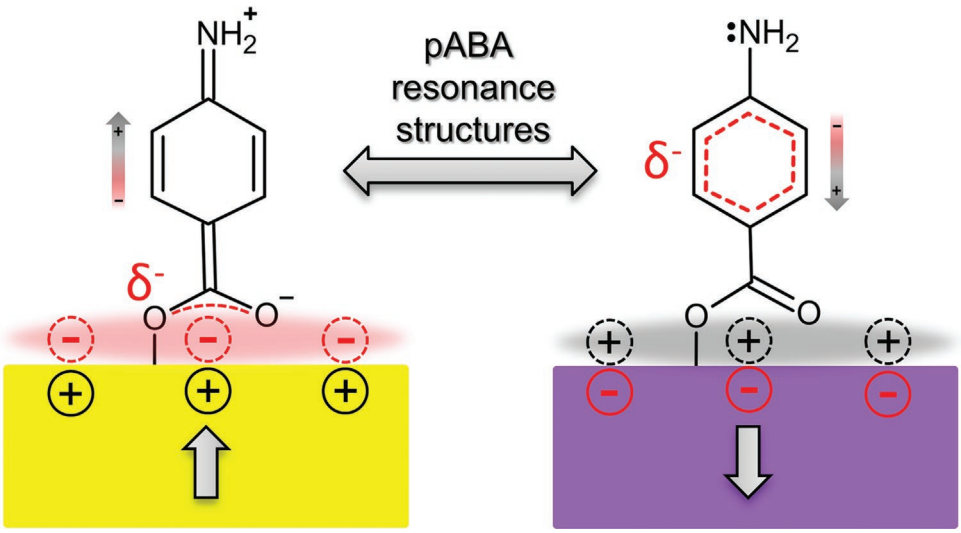

Figure 4. Schematic representation of ferroelectric polarization screening mediated by two different pABA resonance structures, with distinct delocalization of electrons. In the case of up-polarized state (left), pABA molecules delocalize electrons from the electro-donating amino group and benzene ring towards the carboxylic group and act as negative screening agents in the vicinity of the surface, making up-polarized state highly stable. Delocalized electrons are represented by red dashed lines. Reversibly, in the case of down-polarized state, all negative charges in the vicinity of the surface are repelled and delocalized inside of the benzene ring. The carboxilic group at the bottom of the molecule thus becomes positively charged, making the down-polarized state highly stable. Thus pABA molecules act as tunable chemical electrodes for bistable ferroelectric polarization screening and stabilization.

2.3. Tunable Electroactive Ferroelectric/pABA/2D Interfaces

An hybrid scenario between conventional electrodes and chemical screening arises with the use of 2D electrodes. Considering graphene as an archetypal 2D electrode material,[12,19] it is hard to control the interface composition and the presence of intercalated molecules due to the transfer process of the graphene itself and also due the ubiquitous presence of surface adsorbates on ferroelectric surfaces, which moreover strongly depend on the polarization state.[2,4,8,20–22] In turn, this can have an unpredictable effect on the device performance. One way to overcome this issue is the deliberate chemical functionalization of the ferroelectric surface, enabling a controlled interfacial chemical composition: since adsorbates are inevitable, let us at least choose them ourselves so that they work in our favor. As we have just argued in the previous sections, pABA is a promising material in this respect, so the practical question emerges: can we combine the screening ability of pABA molecules with the high in-plane conductivity and mechanical robustness of graphene? In other words, can we intercalate pABA between a graphene electrode and the ferroelectric film, so that the resulting hybrid-electrode capacitor retains the same robust ferroelectricity observed in the pure pABA case?

In this study, we have transferred multilayer (ML) graphene patches obtained by graphite exfoliation to pABA-functionalized BTO thin films, in order to build hybrid organic–ferroelectric capacitor-like structures with graphene as the 2D top electrode (**Figure 5**a). Beside other ways for graphene preparation and transfer,[23] mechanical exfoliation[24] was chosen in this work since it doesn't involve contact of the functionalized substrate with any kind of solvents during the graphene transfer and avoids additional chemical modifications that might arise. The 3D topography image of the deposited pABA molecules captured underneath ML graphene patch is presented in Figure 5b.

In order to probe the hysteresis cycle of pABA molecules underneath the graphene patch, an AFM tip was placed in contact with it, as depicted in Figure 5a, while voltage was cycled between –7.5 and 7.5 V. In this configuration, while the electric excitation signal in PFM spreads over the whole graphene electrode, the reading of the electromechanical response is strictly local and only senses the piezoelectric deformation arising below the tip, meaning that the obtained hysteresis cycle corresponds uniquely to that of the graphene(ML)/pABA/BTO/SRO stack under the AFM contact point. The obtained hysteresis loop (Figure 5c) has almost the same characteristics as hysteresis loop measured directly on top of the pABA molecules as shown in Figure 3f. Therefore, the increased coercive field remains when the PFM hysteresis cycles are measured using the ML graphene as top electrode, indicating that pABA molecules are effective buffer layers to stabilize ferroelectric polarization underneath 2D electrodes such as graphene.

3. Conclusions

The resonance properties of pABA molecules (i.e., their distinct configurations of the electronic charge density within the molecule) enable a versatile response to polarization changes in the ferroelectric surface. The chemical bonding between pABA molecules and the BTO surface results in a robust ferroelectric polarization with increased coercive field, thanks to the ability of the pABA molecules to respond to the screening needs of the ferroelectric by internally rearranging its delocalized electrons. Contrary to other chemisorbed species, pABA can tune its surface charge density without having to change the surface bonding. In this way, pABA molecules provide i) controllable and more predictable chemistry of ferroelectric surfaces and ii) agile and effective screening for both polarization states compared to naturally present "unipolar" atmospheric adsorbates.

In addition, pABA's electrons are delocalized only along their vertical axis, and this allows writing ferroelectric domains only in the area under the biased tip, giving them a unique advantage over the conventional metallic electrodes, which distribute the field uniformly across the entire electrode area. Conversely, conventional electrode functionality can be recovered by depositing graphene on top of the pABA layer. The functionalization of ferroelectric interfaces using pABA molecules can therefore be a useful pathway for the stabilization of the polarization in thin film capacitors. This may be of particular interest in the case of ultra-thin films employed in ferroelectric tunnel

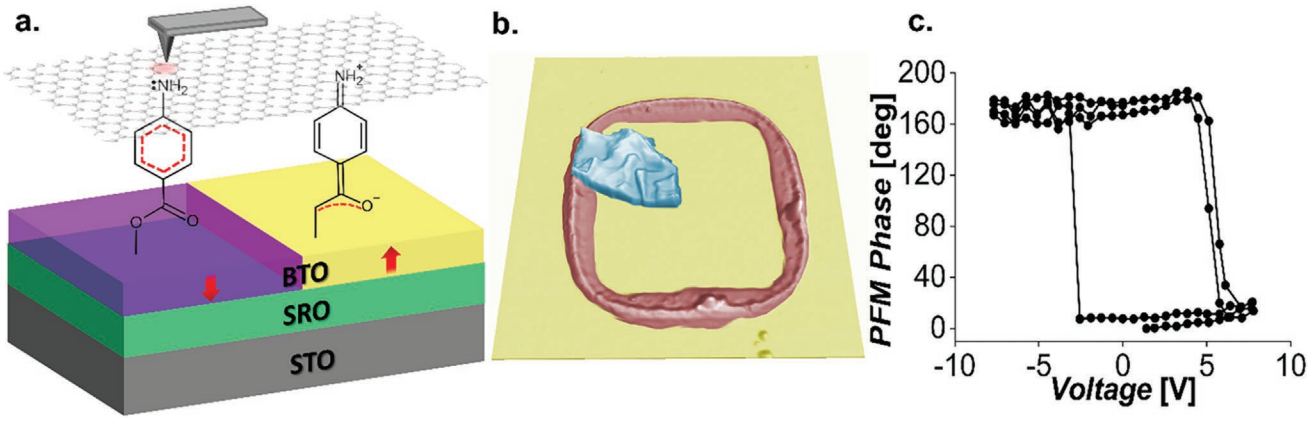

Figure 5. Capacitor structures of graphene(ML)/pABA/BTO/SRO; a) schematic representation of the different electron configurations that pABA molecules are going through during hysteresis loop measurements over capacitor; b) AFM 3D topography of pABA molecules (red) in contact with ML graphene sheet (blue) altogether deposited on BTO thin films (yellow) and c) SS-PFM hysteresis loops measured through ML graphene top electrode, closely resembling those measured directly on pABA molecules.

junctions, whereby the polarization stability of ultra-thin films could be enhanced. Altogether, the obtained results have a strong impact in the field of interface engineering of nanodevices, whereby hybrid interfaces can be designed to tune the overall device performance.

4. Experimental Section

$SrRuO_3$(SRO)/$BaTiO_3$ (BTO) Thin Film Preparation: Structural properties of as-grown BTO thin films were studied by X-Ray diffraction in theta/2theta ($\theta/2\theta$) geometry, whereby θ and 2θ denote incident and diffracted angle, respectively. Coupled $\theta/2\theta$ scans and X-Ray reciprocal space map (XRSM) measurements were performed on PANalytical X'Pert Pro diffractometer. Results of structural characterization of BTO/SRO bilayers are presented in Supporting Information.

Microcontact Printing (μCP): Surface functionalization was achieved by microcontact printing. Polymeric PDMS stamps created by a curing process at elevated temperatures were used, which have opposite features to the master template made of silica. Once cured, stamp was peeled off and cut to necessary size. In the experiments, 1 cm × 1 cm PDMS stamps were used with square-like features of 5 μm × 5 μm separated by 10 μm. PDMS stamp was inked with 0.1 M pABA solution (pABA, purified by sublimation, ≥ 99%, Sigma–Aldrich) in gamma-butyrolactone (GBL, reagentplus ≥ 99%, Sigma–Aldrich) solvent by spreading 200 μl droplet of solution over it. This step was necessary in order to let pABA molecules adsorb onto the PDMS stamps. After 20 min, pABA solution was removed from PDMS surface and slightly dried using N_2 flow. The PDMS stamp was then placed in conformal contact with the BTO thin film during 15 min, after which it was carefully separated from the BTO substrate. After functionalization, the BTO thin film was subjected to thermal annealing on a hot plate at 80 °C during 30 min in order to evaporate the solvent. Since pABA is hygroscopic, all reagents were stored and later used for solution preparation inside of a controlled humidity glove box.

Graphene Electrodes Deposition onto pABA-Functionalized BTO Surfaces: In order to build hybrid organic ferroelectric capacitor-like structures, ML graphene sheets were used with thickness of about 10–20 nm obtained by mechanical exfoliation of highly oriented pyrolytic graphite (HOPG, SPI Supplies) with adhesive tape. During this process, normal force was exerted on the HOPG surface in order to overcome the van der Waals attraction forces and to micromechanically cleave graphite sheets. Achieving very thin layers required several exfoliation steps. After exfoliation, the obtained multilayer graphene sheets were deposited onto pABA-functionalized BTO and used as top electrodes for PFM characterization.

Atomic Force Microscopy (AFM) Measurements: AFM imaging was performed on MFP-3D AFM (Asylum Research). In all the experiments, $PtIr_5$ coated PPP-EFM tips (Nanosensors) with a stiffness constant k = 2.8 N/m were used. The topography of the samples was imaged in tapping mode, while in order to investigate ferroelectric, electronic and mechanical properties of bare and functionalized thin films at the nano scale, different AFM modes were employed such as Piezoresponse Force Microscopy (PFM), Kelvin Probe Force Microscopy (KPFM) or Multifrequency AFM imaging[25] (MF-AFM) like AM-FM viscoelastic mapping.

In the PFM mode, an AC voltage was applied to a conductive AFM tip used as top mobile electrode and then scanned over the surface in contact mode. The PFM amplitude image of the mechanical vibration of the tip was proportional to the magnitude of the electromechanical response of the sample, while the PFM phase gave information about the orientation of ferroelectric polarization in the material.

In AM-FM Viscoelastic Mapping fundamental resonance frequency f_1 was operated in amplitude modulation mode (AM) to track the topography, while the second eigenmode frequency f_2 was operated in frequency modulated mode (FM). In this case amplitude of the second eigenmode A_2 was kept constant by adjusting driving voltage, while the frequency f_2 was adjusted in order to keep phase φ_2 at °90. Changes in amplitude of the second eigenmode A_2 and supplied driving voltage contained information about energy dissipation, while changes in the frequency f_2 bear information about elastic tip-sample interaction. Using obtained information about amplitude, phase and frequency shift of both modes quantitative data such as stiffness, elasticity, dissipation and Young's modulus could be extracted. It was important to notice that AM-FM Viscoelastic mapping was intermittent-contact mode and was therefore very useful, non-invasive technique for obtaining information about chemical and/or mechanical properties of functionalized samples with high lateral resolution. In this case the value of fundamental resonance frequency was $f_1 = 71.8$ kHz and that of the second eigenmode $f_2 = 457.0$ kHz, giving correct relationship of $f_2/f_1 = 6.4$ for the application of this AFM mode.

Finally, KPFM measurements were employed to study the electronic structure of bare and pABA-functionalized BTO surfaces. Measurements were conducted in two-pass mode. In the first pass topography information was obtained, while in the second pass DC voltage was applied to the tip in order to compensate electric potential between tip and the sample and to cancel vibration of the cantilever. The obtained DC voltage represented contact potential difference (CPD) between tip and the sample.

Supporting Information

Supporting Information is available from the Wiley Online Library or from the author.

Acknowledgements

The authors acknowledge N. Aliaga-Alcalde and A. Verdaguer for providing with the PDMS stamps and Prof. M. Lira and Dr. H. Xie for providing the molecules. Financial support was obtained under projects from the Spanish Ministerio de Ciencia e Innovacion (MICINN) under projects PID2019-108573GB- C21 and PID2019-109931GB-I00. In addition, this work was partially funded by 2017-SGR-579 from the Generalitat de Catalunya. The ICN2 was funded by the CERCA programme / Generalitat de Catalunya. The ICN2 was supported by the Severo Ochoa Centres of Excellence Programme, funded by the Spanish Research Agency (AEI, grant no. SEV-2017-0706). I.S. acknowledges support of the Secretaria d'Universitats i Recerca – Departament d'Empresa i Coneixement – Generalitat de Catalunya and the European Social Fund (ESF) (FI grant reference 2020 FI_B2 00157).

Conflict of Interest

The authors declare no conflict of interest.

Data Availability Statement

The data that support the findings of this study are available from the corresponding author upon reasonable request.

Keywords

$BaTiO_3$ ferroelectric thin films, chemical electrodes, graphene ferroelectric capacitors, molecular functionalization, para-aminobenzoic acid (pABA) molecules, polarization screening

Received: December 20, 2022
Revised: February 27, 2023
Published online: April 17, 2023

[1] J. J. Segura, N. Domingo, J. Fraxedas, A. Verdaguer, *J. Appl. Phys.* **2013**, *113*, 187213.
[2] N. Domingo, E. Pach, K. Cordero-Edwards, V. Pérez-Dieste, C. Escudero, A. Verdaguer, *Phys. Chem. Chem. Phys.* **2019**, *21*, 4920.
[3] J. L. Wang, F. Gaillard, A. Pancotti, B. Gautier, G. Niu, B. Vilquin, V. Pillard, G. L. M. P. Rodrigues, N. Barrett, *J. Phys. Chem. C* **2012**, *116*, 21802.
[4] I. Spasojevic, G. Sautier, J. Caicedo, A. Verdaguer, N. Domingo, *Appl. Surf. Sci.* **2021**, *565*, 150288.
[5] R. V. Wang, D. D. Fong, F. Jiang, M. J. Highland, P. H. Fuoss, C. Thompson, A. M. Kolpak, J. A. Eastman, S. K. Streiffer, A. M. Rappe, G. B. Stephenson, *Phys. Rev. Lett.* **2009**, *102*, 2.
[6] P. Zubko, H. Lu, C. W. Bark, X. Martí, J. Santiso, C. B. Eom, G. Catalan, A. Gruverman, *J Phys Condens Matter* **2017**, *29*, 284001.
[7] R. P. Dahl-Hansen, J. M. Polfus, E. Vøllestad, B. Akkopru-Akgun, L. Denis, K. Coleman, F. Tyholdt, S. Trolier-Mckinstry, T. Tybell, *J. Appl. Phys.* **2020**, *127*, 244101.
[8] N. Domingo, I. Gaponenko, K. Cordero-Edwards, N. Stucki, V. Pérez-Dieste, C. Escudero, E. Pach, A. Verdaguer, P. Paruch, *Nanoscale* **2019**, *11*, 17920.
[9] J. Shin, V. B. Nascimento, G. Geneste, J. Rundgren, E. W. Plummer, B. Dkhil, S. V. Kalinin, A. P. Baddorf, *Nano Lett.* **2009**, *9*, 3720.
[10] M. J. Highland, T. T. Fister, M. I. Richard, D. D. Fong, P. H. Fuoss, C. Thompson, J. A. Eastman, S. K. Streiffer, G. B. Stephenson, *Phys. Rev. Lett.* **2010**, *105*, 167601.
[11] Y. Tian, L. Wei, Q. Zhang, H. Huang, Y. Zhang, H. Zhou, F. Ma, L. Gu, S. Meng, L.-Q. Chen, C.-W. Nan, J. Zhang, *Nat. Commun.* **2018**, *9*, 3809.
[12] H. Lu, A. Lipatov, S. Ryu, D. J. Kim, H. Lee, M. Y. Zhuravlev, C. B. Eom, E. Y. Tsymbal, A. Sinitskii, A. Gruverman, *Nat. Commun.* **2014**, *5*, 5518.
[13] P. Vollhardt, N. E. Shore, *Organic Chemistry: Structure and Function*, W.H. Freeman & Co. Ltd, New York **2014**.
[14] A. P. Cismesia, G. R. Nicholls, N. C. Polfer, *J. Mol. Spectrosc.* **2017**, *332*, 79.
[15] L. Pauling, *J. Am. Chem. Soc.* **1931**, *53*, 3225.
[16] S. Yang, Y. Ishikawa, H. Itoh, Q. Feng, *J. Colloid Interface Sci.* **2011**, *356*, 734.
[17] B. Li, Y. Chen, Z. Liang, D. Gao, W. Huang, *RSC Adv.* **2015**, *5*, 94290.
[18] P. Zubko, D. J. Jung, J. F. Scott, *J. Appl. Phys.* **2006**, *100*, 114112.
[19] H. Lu, B. Wang, T. Li, A. Lipatov, H. Lee, A. Rajapitamahuni, R. Xu, X. Hong, S. Farokhipoor, L. W. Martin, C.-B. Eom, L.-Q. Chen, A. Sinitskii, A. Gruverman, *Nano Lett.* **2016**, *16*, 6460.
[20] T. Li, A. Lipatov, H. Lu, H. Lee, J.-W. Lee, E. Torun, L. Wirtz, C.-B. Eom, J. Íñiguez, A. Sinitskii, A. Gruverman, *Nat. Commun.* **2018**, *9*, 3344.
[21] T. Li, P. Sharma, A. Lipatov, H. Lee, J. W. Lee, M. Y. Zhuravlev, T. R. Paudel, Y. A. Genenko, C. B. Eom, E. Y. Tsymbal, A. Sinitskii, A. Gruverman, *Nano Lett.* **2017**, *17*, 922.
[22] Y. Li, X. Y. Sun, C. Y. Xu, J. Cao, Z. Y. Sun, L. Zhen, *Nanoscale* **2018**, *10*, 23080.
[23] S. Ullah, X. Yang, H. Q. Ta, M. Hasan, A. Bachmatiuk, K. Tokarska, B. Trzebicka, L. Fu, M. H. Rummeli, *Nano Res.* **2021**, *14*, 3756.
[24] K. S. Novoselov, A. K. Geim, S. V. Morozov, D. Jiang, Y. Zhang, S. V. Dubonos, I. V. Grigorieva, A. A. Firsov, *Science* **2004**, *306*, 666.
[25] R. Garcia, E. T. Herruzo, *Nat. Nanotechnol.* **2012**, *7*, 217.